

# Photovoltaic Model Parameters Identification Using an Improved Artificial Lemming Algorithm

Ling-Long Tan, Qi-Jian Wang\*, and Qing Wang

School of Electronics Engineering, Anhui Xinhua University,  
Hefei, China

[tanlinglong@axhu.edu.cn](mailto:tanlinglong@axhu.edu.cn), [wangqijian@axhu.edu.cn](mailto:wangqijian@axhu.edu.cn), [wangqing@axhu.edu.cn](mailto:wangqing@axhu.edu.cn)

*Received 26 May 2025; Revised 2 June 2025; Accepted 2 June 2025*

**Abstract.** As a clean and renewable resource, solar energy offers a significant advantage over nonrenewable energy sources due to its abundance. Photovoltaic (PV) systems represent a promising technology for the direct conversion of sunlight into direct current electricity. Identifying PV model parameters is a complex nonlinear optimization problem. Traditional metaheuristic algorithms often encounter several challenges. They may converge slowly, get stuck in local optima, or require complex parameter tuning to perform well. In response to these challenges, this study proposes a novel parameter estimation technique, IALA. It combines the Artificial Lemming Algorithm (ALA) with a triangular walking strategy and an inverse cumulative Cauchy distribution operator. The triangular walking strategy enhances the exploration ability of ALA and reduces the risk of getting trapped in local optima. At the same time, the inverse cumulative Cauchy distribution operator strengthens its exploitation mechanism, accelerating convergence toward the optimal solution. The proposed algorithm is used to estimate the optimal parameters of single-, dual-, triple-, four-diode PV models and compared with several existing well-established algorithms. Systematic comparisons over 100 independent runs, the improved ALA (IALA) performs better than other techniques. It provides more accurate and robust parameter estimation for various PV models. Furthermore, its robustness is validated through statistical assessments, including the wilcoxon signed-rank test.

**Keywords:** artificial lemming algorithm, Cauchy inverse cumulative distribution operator, triangular walking strategy, photovoltaic models, parameter estimation

## 1 Introduction

The growing need for clean energy and the pressing need to reduce environmental pollution have led to a sharp increase in the popularity of solar energy, one of the most promising renewable resources. Photovoltaic (PV) technology is central to this transition. It enables the direct conversion of sunlight into electrical energy. To maximize their performance and efficiency, accurate parameter modeling is essential. Precise identification of PV model parameters enables reliable performance prediction, cost-effectiveness analysis, and system optimization under various operating conditions [1].

A range of methods, including analytical, direct, numerical, and conventional optimization-based approaches, have been investigated by researchers in an attempt to identify the critical parameters of photovoltaic (PV) models. Constraints imposed on the objective function, however, often limit the applicability and effectiveness of these methods. To overcome these challenges, swarm intelligence (SI) algorithms have gained prominence, as they can efficiently approximate optimal solutions within a reasonable computational time. As a result, SI algorithms have gained a lot of interest and been effectively used in the energy conversion industry.

Saleem et al. (2009) proposed an analytical method using four points of the J-V curve. However, it is only applicable under ideal conditions [2]. Maouhoub (2018) employed the least squares method for I-V curve fitting, demonstrating sensitivity to noise interference [3]. Di Piazza et al. (2013) developed a dynamic parameter identification method using least-squares regression, showing effectiveness in time-varying environments [4]. While these mathematically-derived solutions offer computational efficiency, their performance remains highly dependent on initial values.

---

\* Corresponding Author

Jordehi (2016) introduced time-varying acceleration coefficient PSO (TVACPSO), effectively balancing exploration and exploitation capabilities [5]. Abido et al. (2018) achieved seven-parameter PV model identification with rapid convergence, albeit requiring careful parameter tuning. However, its sensitivity to parameter tuning and dependence on manufacturer data limit its robustness in noisy or dynamic environments [6]. In genetic algorithm developments, Bendaoud et al. (2019) combined GA with simulated annealing to address multimodal optimization challenges [7]. However, dependence on experimental I-V data constrains its use in dynamic or large-scale PV systems requiring real-time identification. While these global optimization algorithms show promise, they remain prone to local optima convergence.

Merchaoui et al. (2018) significantly improved shading condition performance through adaptive mutation in PSO. However, its heavy reliance on mutation strategy design increases algorithmic complexity and limits generalizability across problem domains [8]. Ridha et al. (2020) enhanced the Harris Hawks Optimizer (HHO) with mutation operators. This improvement helps the single-diode model avoid getting trapped in local optima. Despite improved convergence, the algorithm remains fragile to initial condition variations and degrades significantly in noisy or dynamic settings [9]. Oliva et al. (2017) incorporated chaotic mapping into the whale optimization algorithm (WOA), which can enhance the robustness of the dual diode model [10]. Elazab et al. (2018) successfully applied WOA for both single and multiple diode model parameter identification. Nevertheless, WOA often converges slowly in later stages and is sensitive to the exploration-exploitation balance [11].

Long et al. (2020) incorporated the Cuckoo Search (CS) algorithm into the Grey Wolf Optimizer (GWO), demonstrating enhanced performance in parameter extraction under complex lighting conditions. However, the hybrid algorithm involves multiple control parameters from both CS and GWO, increasing implementation complexity and requiring careful tuning to ensure stability and convergence efficiency [12]. Chen et al. (2020) incorporated chaotic drift strategies into Harris Hawks Optimization (HHO), effectively improving precision for three-diode PV models. Nonetheless, the added diversification mechanisms may increase computational overhead. The performance of the method may also degrade in high-dimensional or time-sensitive applications due to slower convergence in the later stages [13]. Zhang et al. (2020) proposed a new algorithm that combines the orthogonal Nelder-Mead simplex method with the Moth Flame optimizer (MFO), which significantly reduced computational cost while maintaining high accuracy. Yet, the hybrid structure may limit flexibility across different PV model types, and its search capability can be sensitive to initial solution distribution [14]. These approaches effectively combine multiple algorithmic advantages to overcome individual method limitations.

Sundareswaran et al. (2015) proposed a new algorithm, the artificial bee colony (ABC) algorithm, which can be used to track the global maximum power point (GMPP) under non-uniform insolation conditions. While effective in handling partial shading, the algorithm may suffer from premature convergence and reduced tracking accuracy under rapidly changing irradiance [15]. These studies address practical implementation challenges and complex model scenarios.

This study presents an improved Artificial Lemming Algorithm (ALA). It incorporates a triangular walking strategy and an inverse cumulative Cauchy distribution operator. The algorithm effectively improves the accuracy and consistency of photovoltaic (PV) module parameter estimation. The improved ALA algorithm (IALA) is evaluated against state-of-the-art optimization methods on four different PV parameter identification problems. Experimental results show that IALA achieves superior accuracy and reliability with lower computational requirements compared to existing approaches. The principal contributions of this work include:

In summary, the contributions of this article are as follows:

(1) We propose an improved Artificial Lemming Algorithm (IALA) that integrates a triangular walking strategy and an inverse cumulative Cauchy distribution operator. This enhancement improves the local search capability of the swarm for identifying optimal solutions and accelerates convergence. It is specifically designed for photovoltaic system parameter extraction.

(2) Through extensive experiments, this paper validates the performance of IALA across single-, double-, triple-, and quadruple-diode photovoltaic models, demonstrating its superiority over the most advanced algorithms currently in use.

## 2 Photovoltaic Models

In this section, mathematical representations of four PV models—ranging from one-diode to four-diode configurations—that characterize the nonlinear behavior of output current in photovoltaic systems. By analyzing

these mathematical representations, this study aims to enhance the understanding of how output current responds to varying environmental conditions.

## 2.1 Single Diode Model

The single diode model (SDM) equivalent circuit consists of a parallel diode, two resistors representing series and shunt effects, and a current source. This is shown in Fig. 1(a). Equation (1) provides the output current of the SDM [16].

$$i_{out} = i_{photo} - i_d - i_{shunt} . \quad (1)$$

Here,  $i_{photo}$  is the photo-generated current induced by solar irradiation, and  $i_{out}$  is the net output current delivered by the photovoltaic cell. The diode current,  $i_d$  is computed using Equation (2) based on the Shockley equation. In Equation (3),  $i_{shunt}$  contributes to the overall current path of the model and represents the current flowing through the shunt resistor.

$$i_d = i_{sd} \left( \exp \left( \frac{q(i_{out} R_s + V_{out})}{nkT} \right) - 1 \right) . \quad (2)$$

$$i_{shunt} = \frac{(i_{out} R_s + V_{out})}{R_{shunt}} . \quad (3)$$

In this case,  $q$  is  $1.60217646 \times 10^{-19} C$ , representing the charge of the electron,  $V_{out}$  is the output voltage of the photovoltaic cell, and  $n$  is the ideality factor of the diode.  $R_s$  and  $R_{sh}$ , respectively, equal the series and shunt resistances.  $i_{sd}$  is the reverse saturation current of the diode,  $k$  is the Boltzmann constant, and  $T$  is the Kelvin temperature of the P-N junction.

## 2.2 Double Diode Model

Fig. 1(b) shows the equivalent circuit of the Double Diode Model (DDM), which is used to determine the load current. The DDM is given by the following Equations [17].

$$i_{out} = i_{photo} - i_{d1} - i_{d2} - i_{shunt} . \quad (4)$$

$$i_{d1} = i_{sd1} \left( \exp \left( \frac{q(i_{out} R_s + V_{out})}{n_1 kT} \right) - 1 \right) . \quad (5)$$

$$i_{d2} = i_{sd2} \left( \exp \left( \frac{q(i_{out} R_s + V_{out})}{n_2 kT} \right) - 1 \right) . \quad (6)$$

Where  $\{i_{d1}, i_{d2}\}$  stands for the diode currents of the P-N junctions,  $\{i_{sd1}, i_{sd2}\}$  indicate the P-N junctions saturation currents, The ideality factors of the P-N junctions are denoted as  $n_1$  and  $n_2$ .  $i_{shunt}$  can be obtained from Equation (3).

## 2.3 Triple Diode Model

The corresponding circuit for the three-diode model is depicted in Fig. 1(c). It includes two resistors, three diodes, and a current source. Nine parameters need to be determined from the measured I-V data of the solar cell in order to use this model. The nine unknown parameters are  $R_s$ ,  $R_{sh}$ ,  $i_{photo}$ ,  $i_{sd1}$ ,  $i_{sd2}$ ,  $i_{sd3}$ ,  $n_1$ ,  $n_2$  and  $n_3$ .  $i_{out}$ ,

$i_{photo}$ ,  $i_{shunt}$  and  $i_d$ , respectively, define the cell output current, photo-generated current, diode current, and shunt resistor current. Additionally,  $n$  represents the ideality factor and  $R_{sh}$  represents the parallel circuit resistance, and the series resistance by  $R_S$  in the shunt resistor current. Equation 7 defines the output current of the three-diode model. The diffusion, saturation, and leakage currents are represented by  $i_{d1}$ ,  $i_{d2}$  and  $i_{d3}$  in Equation 5, Equation 6, and Equation 8, respectively. Equation (3) can be used to obtain  $i_{shunt}$ .  $n_1$ ,  $n_2$  and  $n_3$  stand for the diffusion and recombination diode ideality factors [18, 19].

$$i_{out} = i_{photo} - i_{d1} - i_{d2} - i_{d3} - i_{shunt} . \quad (7)$$

$$i_{d3} = i_{sd3} \left( \exp \left( \frac{q(i_{out} R_S + V_{out})}{n_3 k T} \right) - 1 \right) . \quad (8)$$

## 2.4 Four Diode Model

In Fig. 1(d), the four diode model is shown. The following equations can be used to characterize the FDM. The values of  $i_{d1}$ ,  $i_{d2}$ ,  $i_{d3}$ , and  $i_{shunt}$  are obtained from Equations (5), (6), (8), and (3), respectively [20].

$$i_{out} = i_{photo} - i_{d1} - i_{d2} - i_{d3} - i_{d4} - i_{shunt} . \quad (9)$$

$$i_{d4} = i_{sd4} \left( e^{q(V_{out} + i_{out} R_S) / n_4 k T} - 1 \right) . \quad (10)$$

where  $n_4$  is the ideality factor of the P-N junction. The reverse saturation current is denoted by  $i_{sd4}$  and the diode current by  $i_{d4}$ . The FDM and model TDM have the same other parameters.

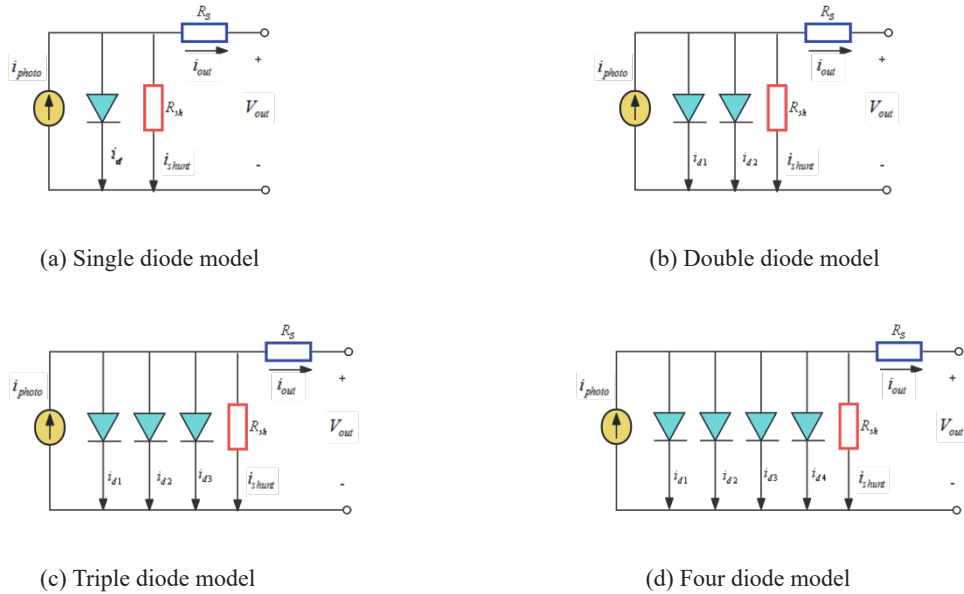


Fig. 1. The equivalent circuit

## 2.5 Objective Function

Minimizing the target function derived from a real-world model is the primary objective of most optimization issues. Therefore, it is essential to formulate an objective function that is both accurate and computationally

efficient. Finding the ideal model parameters is crucial to reducing the difference between measured and computed current levels. The objective function is defined by Equation (11) as the root mean square error (RMSE) [21].

$$RMSE(X) = \sqrt{\frac{1}{M} \sum_{i=1}^M \left( i_{photo} - i_{sd} \left( \exp \left( q \left( \frac{i_{out} R_s + V_{out}}{nkT} \right) - 1 \right) - \frac{i_{out} R_s + V_{out}}{R_{sh}} - i_{out} \right)^2 \right)}. \quad (11)$$

Let  $M$  denote the total number of measured current samples. The experimentally acquired data is represented by the output voltage  $V_{out}$  and current  $i_{out}$ . An essential indicator for assessing the consistency of the current algorithm is the  $RMSE$ . To put it another way, a lower  $RMSE$  number shows greater algorithmic consistency because it shows that the simulated data the algorithm produced closely matches the observed values.

### 3 Related Works

#### 3.1 Artificial Lemming Algorithm

The four unique behaviors of lemmings served as the inspiration for the Artificial Lemming Algorithm (ALA) proposed by Yaning Xiao et al. [22]. The corresponding mathematical formulations are subsequently introduced.

##### (1) Long-distance migration

The first behavior models lemmings exploring the search space based on their current position and the positions of randomly selected individuals in the population. This strategy helps them identify habitats rich in food resources, enhancing their living conditions. Notably, the direction and distance of their migration are dynamic and influenced by various factors, such as ecological conditions. The following formula is proposed to model this behavior:

$$X_i(t+1) = X_{optimal}(t) + S_{flag} \times B_M \times (R \times (X_{optimal}(t) - X_i(t)) + (1-R) \times (X_i(t) - X_a(t))). \quad (12)$$

At iteration  $t+1$ ,  $X_{optimal}(t)$  represents the location of the  $i^{th}$  search agent, and  $X_i(t+1)$  represents the current optimal solution. According to Equation (19), the parameter  $S_{flag}$  controls the direction of the search by acting as a flag. This mechanism helps avoid local optima and increases the likelihood of thoroughly exploring the problem domain. The sign  $B_M$  stands for a vector of random numbers that represents Brownian motion. Equation (18) defines the standard Brownian motion. Equation (20) generates  $R$ , a  $1 \times DIM$  vector whose elements are uniformly distributed random integers within the interval  $[-1, 1]$ .  $X_a(t)$  is a randomly selected search agent from the population, and  $\alpha$  is an integer index that ranges from 1 to  $N$ , and  $X_i(t)$  reflects the current position of the  $i^{th}$  search agent.

$$f_{B_M}(x; 0, 1) = \frac{e^{-x^2/2}}{\sqrt{2\pi}}. \quad (13)$$

$$S_{flag} = \begin{cases} 1, & \lfloor 2 \times R_{rand} + 1 \rfloor = 1 \\ -1, & \lfloor 2 \times R_{rand} + 1 \rfloor = 2 \end{cases}. \quad (14)$$

$$R = 2 \times R_{rand}(1, DIM) - 1. \quad (15)$$

##### (2) Digging holes

Lemmings randomly dig new burrows. This is based on their current burrow position and the locations of randomly selected individuals in the population. The behavior is modeled by Equation (16).

$$X_i(t+1) = X_i(t) + S \times L_{rand} \times (X_{best}(t) - X_b(t)) . \quad (16)$$

Here,  $b$  is a random integer index between 1 and  $N$ , whereas  $X_b$  denotes a search agent selected at random from the population. When lemming individuals dig a new burrow, their interactions are described using  $L_{rand}$  and  $X_b$ . The value of  $L_{rand}$  is determined using the formula below:

$$L_{rand} = \left( \sin\left(\frac{1}{2}t\right) + 1 \right) \times R_{rand} . \quad (17)$$

### (3) Foraging for food

To maximize food intake, lemmings randomly wander within their foraging area. To model this stage, the spiral wrapping mechanism is used, as explained below:

$$X_i(t+1) = X_{optimal}(t) + S_{flag} \times screw \times R_{rand} \times X_i(t) . \quad (18)$$

Here,  $screw$  stands for a spiral pattern of haphazard foraging search, as defined by Equations (19) and (20).

$$screw = \left( \sin(2\pi \times R_{rand}) + \cos(2\pi \times R_{rand}) \right) \times Radius . \quad (19)$$

$$Radius = \sqrt{\sum_{j=1}^{DIM} (x_{optimal,j}(t) - x_{i,j}(t))^2} . \quad (20)$$

Here, the Euclidean distance between the existing site and the ideal solution is known as the foraging scope, or  $Radius$ .

### (4) Evading natural predators

Lemmings use their exceptional running skills to flee to their burrow as soon as they detect an enemy. The corresponding mathematical expression is depicted in Equation (21).

$$X_i(t+1) = X_{optimal}(t) + S_{flag} \times \varphi \times levy(DIM) \times (X_{optimal}(t) - X_i(t)) . \quad (21)$$

$$\varphi = 2 \times \left( 1 - \frac{t}{t_{max}} \right) . \quad (22)$$

$\varphi$  represents the escape coefficient of lemmings, indicating their ability to evade threats. This capability decreases as the iteration count increases, as defined in Equation (22).  $t_{max}$  indicates the maximum number of iterations. The escape strategies employed by lemmings are mathematically modeled using the Lévy flight function, also referred to as the  $levy$  distribution. The following is the formulation of the Lévy flight function:

$$levy(x) = \frac{\alpha \times v \times 0.01}{|\gamma|^{\frac{1}{\beta}}} , \quad v = \left( \frac{\Gamma(1+\beta) \times \sin \frac{\pi\beta}{2}}{\Gamma\left(\frac{(1+\beta)}{2}\right) \times \beta \times 2^{\left(\frac{(\beta-1)}{2}\right)}} \right)^{\frac{1}{\beta}} . \quad (23)$$

$\alpha$  and  $\gamma$  are random numbers between 0 and 1, but  $\beta$  is a constant set to 1.5.

### (5) Transition from exploration to exploitation

Lemmings migrate or burrow preferentially when they have enough energy, but otherwise they forage and avoid predators. The energy factor is calculated using the following formula:

$$E(t) = 4 \ln \left( \frac{1}{R_{rand}} \right) \times \arctan \theta, \quad \theta = \left( 1 - \frac{t}{t_{max}} \right). \quad (24)$$

Equation (25) evaluates the probability that  $E > 1$ .

$$P\{E(t) > 1\} = \int_0^1 \int_0^{e^{-\frac{1}{4 \arctan \delta}}} \frac{dr d\delta}{1} \Rightarrow y = -\frac{1}{4 \arctan \delta}, \int_{-\infty}^{\frac{1}{\pi}} e^y \frac{1}{4y^2 \cos^2 \left( \frac{1}{4y} \right)} dy \approx 0.5060. \quad (25)$$

Therefore, if  $E > 1$ , the probability is about 0.5, enabling a smooth shift from exploration to exploitation in the optimizer.

### 3.2 Triangular Walking Strategy

In the exploration stage of the ALA algorithm, a triangular walking strategy is introduced to increase search diversity and improve exploration. This method is founded on the relationship between the current and the best known solutions. By performing random movements within a virtual triangle, this strategy allows fine-grained searches in neighbouring regions of the problem space, thus increasing the probability of identifying local optima. When lemmings conduct intensive searches in a specific region, the triangular walking strategy facilitates exploration in adjacent areas, potentially leading to further solution refinement. This approach helps optimize solution quality in the vicinity of already identified high-quality solutions [23]. The following is the relevant mathematical formulation.

$$X(t+1) = rR + X_{optimal}(t). \quad (26)$$

$$R = L^2 + L_r^2 - 2LL_r \cos 2\pi r. \quad (27)$$

$$L = X_{optimal}(t) - X_i(t). \quad (28)$$

$$L_r = rL. \quad (29)$$

The variable  $X_{optimal}(t)$  denotes the optimal position of a lemming at time  $t$ , while  $X_i(t)$  represents its current position at time  $t$ .  $X(t+1)$  stands for the set of new positions at the subsequent time step.  $L$  represents the distance between the lemming and its prey, the parameter  $L_r$  denotes the step size in the movement of a lemming,  $R$  is a parameter computed based on the triangular walking strategy, and  $r$  is a number that is generated at random within the range  $[0,1]$ .

After revision, Equation (12) is now shown as follows.

$$X'_i(t+1) = X_i(t+1) + r \times R. \quad (30)$$

### 3.3 Inverse Cumulative Cauchy Distribution Operator

The cumulative distribution function of a continuous probability distribution, the Cauchy distribution, is shown in the following statement [24].

$$f(x) = \frac{1}{\pi} \arctan\left(\frac{x-\mu}{\gamma}\right) + \frac{1}{2}. \quad (31)$$

The corresponding inverse function is given by:

$$f(x)^{-1} = a + b \tan(\pi(r1 - 0.5)). \quad (32)$$

In the equation,  $\mu$  denotes the location parameter, representing the median of the distribution and is set to 0,  $r1$  is a random number in the interval  $[0,1]$ . The scale parameter  $\gamma$ , which controls the width of the distribution, is set at 0.01.

Equation (21) has been revised and is now updated as follows:

$$X_i(t+1) = S_{flag} \times \varphi \times levy(DIM) \times (X_{optimal}(t) - X_i(t)) + \beta \times \gamma \times \tan\left(\pi\left(p - \frac{1}{2}\right)\right) + X_{optimal}(t). \quad (33)$$

### 3.4 The Proposed IALA Algorithm

The Artificial Lemming Algorithm (ALA) was improved to boost its global exploration, local exploitation, and convergence performance. In the Long-Distance Migration phase, ALA employs a random step-size update strategy, which may lead to a lack of directionality in the search process, thereby affecting global exploration efficiency. To address this issue, a Triangular Walk strategy was introduced in this phase, where the individual positions are adjusted using a uniformly distributed random step size. This approach enables search agents to explore a broader region efficiently while maintaining a degree of randomness, preventing premature convergence to local optima. Adaptability is crucial in the Evading Natural Predators phase for local exploitation in the algorithm. To strengthen local search performance, an inverse cumulative Cauchy distribution operator was implemented. This strategy adaptively adjusts the step size to improve search precision in local regions while maintaining a certain probability of large step jumps, thereby preserving population diversity. Following the above analysis, the recommended IALA pseudocode is shown in the following section, and Fig. 2 displays its flowchart.

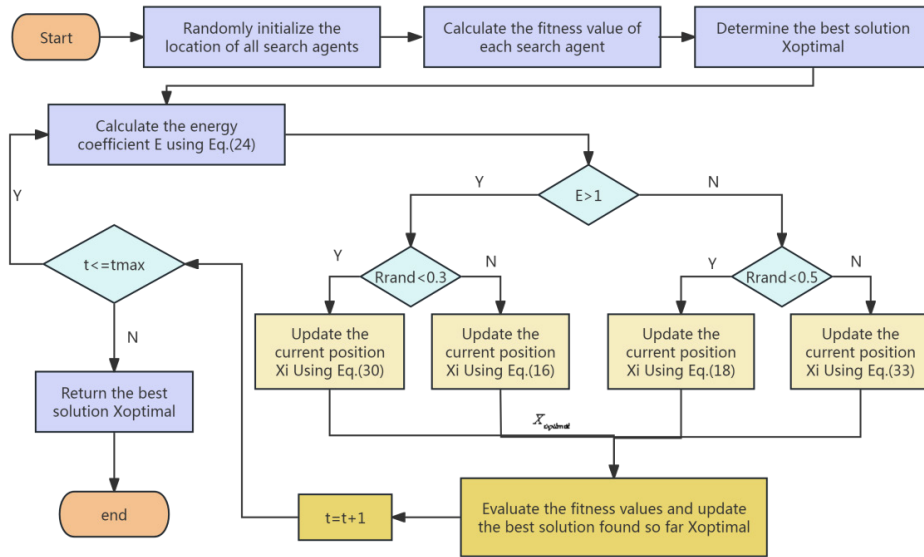


Fig. 2. Flowchart of IALA

---

The pseudocode of IALA

---

Initialization, maximum number of iterations  $Max\_iter$ , population size  $N$ , the location of all lemmings  $X_i$ , ( $i = 1, 2, \dots, N$ ).

Compute the fitness value for each lemming agent in the population.

Record the current optimal solution  $X_{optimal}$

**for** Iter = 1 **to**  $Max\_iter$  **do**;

    The value of  $E$  is computed using Equation (24).

**for** (each search individual  $X_i$ ) **do**

**if** ( $E > 1$ ) **then**

            Exploration phase;

**if** ( $R_{rand} < 0.3$ ) **then**

                Use Equation (30) to update the current location of the lemming.

**else**

                Update the current location of the lemming individual using Equation (16);

**end**

**else**

            Exploitation phase

**if** ( $R_{rand} < 0.5$ ) **then**

                Update the current location of the lemming individual using Equation (18).

**else**

                Use Equation (33) to update the current location of the lemming.

**end**

**end**

**end**

    Recalculate fitness values of all lemming individuals

    Update the best solution that has been found thus far,  $X_{optimal}$

    Iter = Iter + 1;

**end**

---

## 4 Experimental Results and Analysis

In this section, the proposed IALA algorithm is applied to the parameter estimation of four photovoltaic models.

The experimental data used 26 current/voltage measurements from a French RTC solar cell with a diameter of 57 mm, operating at 33°C and a power density of 1000 W/m<sup>2</sup> [25]. Table 1 shows the parameter ranges for each model. Comparisons are made between the results and those of other algorithms, such as GWO [26], COA [27], GJO [28], DBO [29], HHO [30], and ALA. The maximum number of iterations is set to 100, the population size is 30, and each algorithm is run independently 100 times. The performance and robustness of these methods were evaluated by calculating the standard deviation, best value, mean value, and worst value of these algorithms.

The wilcoxon signed-rank test is used to assess statistical significance and find differences between the proposed algorithm and competing approaches. The difference between the measured and simulated data at each voltage point is measured by the absolute error (IAE).

**Table 1.** The unknown parameter ranges for the different PV models

Parameter	Single/double/Triple/Four-diode model	
	Lower	Upper
$i_{photo}$ (A)	0.00	1.00
$i_{sd1}, i_{sd2}, i_{sd3}, i_{sd4}$ ( $\mu$ A)	0.00	1.00
$R_s$ ( $\Omega$ )	0.00	0.50
$R_{sh}$ ( $\Omega$ )	0.00	100.00
$n, n_2, n_3, n_4$	1.00	2.00

### 4.1 Results on the Single Diode Model

As shown in Table 2, the optimal parameter estimates for each method are listed, accompanied by statistical assessments of the single-diode model using the wilcoxon signed-rank test and RMSE metrics. The bolded outcomes represent the best results. According to the root mean square error in Table 2, the IALA algorithm produc-

es better and more reliable results than the other algorithms. The RMSE distribution over 100 runs is presented in Fig. 3 with a box plot, showing that IALA exhibits high performance stability. The convergence curves of IALA and other enhanced algorithms on the SDM model are displayed in Fig. 4. IALA outperforms the other algorithms in terms of accuracy and convergence speed as the number of evaluations rises.

By comparing the actual values with the estimated values, the absolute error (IAE) for current and power can be calculated. This helps assess the effectiveness of the proposed approach. Table 3 presents the experimentally obtained current and power values along with their corresponding IAE. Table 3 indicates that the current total IAE is  $2.17E-02$ , while that for power is  $8.66E-03$ , indicating a negligible error in power estimation. The results show a strong match between the measured current-voltage and power-voltage data and the SDM model outputs. In Fig. 5, the I-V and P-V curves are displayed, highlighting the excellent performance of the IALA algorithm.

**Table 2.** Results obtained for the SDM

Algorithm		IALA	ALA	GWO	COA	GJO	DBO	HHO
Best -obtained parameters	$i_{photo}(A)$	0.76080	0.76068	0.76084	0.76181	0.76263	0.76089	0.76081
	$i_{sc}(\mu A)$	3.00E-07	2.87E-07	1.70E-07	7.69E-07	6.46E-07	3.43E-07	8.39E-07
	$R_s(\Omega)$	0.03668	0.03686	0.03874	0.03271	0.03437	0.03610	0.03241
	$R_{sh}(\Omega)$	51.84992	52.37447	35.61912	78.07350	87.35788	53.76850	93.84638
	$n$	1.47365	1.46949	1.41891	1.57504	1.55359	1.48727	1.58393
RMSE	Best	<b>9.96E-04</b>	1.02E-03	2.42E-03	3.82E-03	2.82E-03	9.97E-04	2.13E-03
	Worst	<b>6.20E-03</b>	3.82E-02	5.49E-02	2.77E-01	2.23E-01	2.00E-01	8.44E-02
	Mean	<b>2.14E-03</b>	2.95E-03	2.10E-02	1.11E-01	3.58E-02	1.40E-02	2.97E-02
	Std	<b>8.04E-04</b>	5.13E-03	1.52E-02	6.46E-02	2.57E-02	2.57E-02	1.85E-02
wilcoxon-sign			2.17E-11	3.90E-18	3.90E-18	3.90E-18	3.16E-08	3.90E-18

**Table 3.** IAE of IALA on SDM

Item	Measured data		Simulated current data		Simulated power data	
	V (V)	I (A)	$I_{sim}$ (A)	$IAE_I$ (A)	$P_{sim}$ (W)	$IAE_p$ (W)
1	-0.20570	0.76400	0.76422	0.00022	-0.15720	4.60E-05
2	-0.12910	0.76200	0.76275	0.00075	-0.09847	9.66E-05
3	-0.05880	0.76050	0.76139	0.00089	-0.04477	5.25E-05
4	0.00570	0.76050	0.76015	0.00035	0.00433	2.00E-06
5	0.06460	0.76000	0.75901	0.00099	0.04903	6.39E-05
6	0.11850	0.75900	0.75796	0.00104	0.08982	0.00012
7	0.16780	0.75700	0.75698	2.05E-05	0.12702	3.44E-06
8	0.21320	0.75700	0.75600	0.00100	0.16118	0.00021
9	0.25450	0.75550	0.75493	0.00057	0.19213	0.00015
10	0.29240	0.75400	0.75350	0.00050	0.22032	0.00015
11	0.32690	0.75050	0.75123	0.00073	0.24558	0.00024
12	0.35850	0.74650	0.74723	0.00073	0.26788	0.00026
13	0.38730	0.73850	0.74005	0.00155	0.28662	0.00060
14	0.41370	0.72800	0.72740	0.00060	0.30093	0.00025
15	0.43730	0.70650	0.70709	0.00059	0.30921	0.00026
16	0.45900	0.67550	0.67548	1.62E-05	0.31005	7.42E-06
17	0.47840	0.63200	0.63101	0.00099	0.30187	0.00048
18	0.49600	0.57300	0.57216	0.00084	0.28379	0.00042
19	0.51190	0.49900	0.49977	0.00077	0.25583	0.00039
20	0.52650	0.41300	0.41369	0.00069	0.21781	0.00037
21	0.53980	0.31650	0.31743	0.00093	0.17135	0.00050
22	0.55210	0.21200	0.21197	2.76E-05	0.11703	1.52E-05
23	0.56330	0.10350	0.10203	0.00147	0.05747	0.00083
24	0.57360	-0.01000	-0.00886	0.00114	-0.00508	0.00065
25	0.58330	-0.12300	-0.12550	0.00250	-0.07320	0.00146
26	0.59000	-0.21000	-0.20822	0.00178	-0.12285	0.00105
Sum of IAE				2.17E-02		8.66E-03

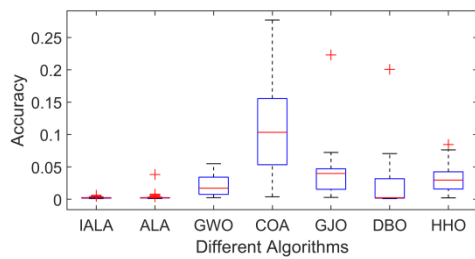


Fig. 3. Box-plot for the single-diode model

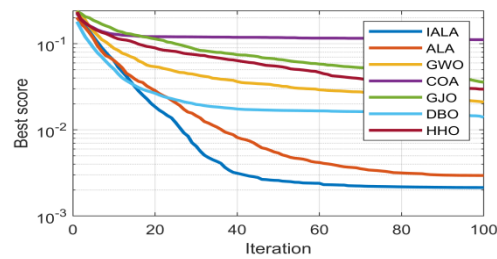


Fig. 4. Convergence performance of IALA and competing algorithms on the SDM model

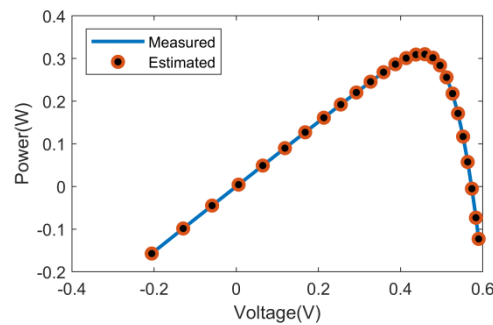
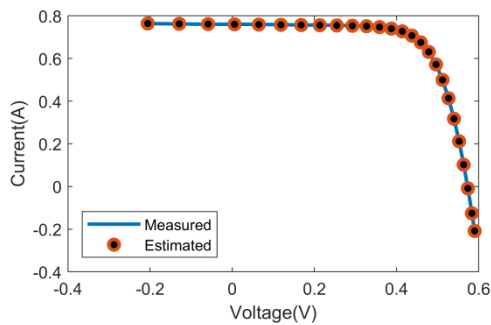


Fig. 5. The I-V and P-V characteristics of the SDM estimated by IALA

### 4.2 Results on the Double Diode Model

The optimization results of the IALA algorithm and other algorithms on the dual-diode model are shown in Table 4. The bolded outcomes are the best. Fig. 6 shows the results of the signed rank test, which also illustrates the accuracy and reliability of the IALA algorithm. Fig. 7 shows the convergence curves of IALA and the comparison algorithms. It can be seen that IALA outperforms other methods in terms of average convergence accuracy. Additionally, IALA exhibits the fastest convergence speed.

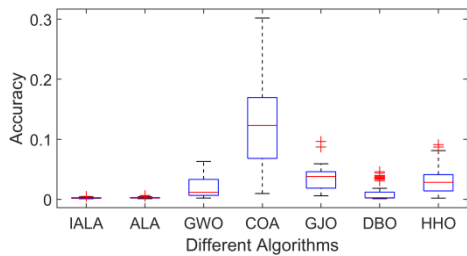
Table 5 gives the differences between the estimated values obtained by the IALA algorithm and the measured values, and gives the IAE values for power and current. For power and current, the total of all IAE values is  $8.97E-03$  and  $2.15E-02$ , respectively. The calculated data and the simulated I-V and P-V curves show a significant correlation, as shown in Fig. 8.

Table 4. Results obtained for the DDM

Algorithm		IALA	ALA	GWO	COA	GJO	DBO	HHO
Best -obtained parameters	$i_{photo}(A)$	0.76069	0.76123	0.75960	0.76959	0.76132	0.76076	0.75849
	$i_{sd1}(\mu A)$	1.00E-06	2.77E-07	4.75E-07	7.79E-07	2.76E-10	3.33E-07	3.85E-07
	$i_{sd2}(\mu A)$	2.11E-07	4.49E-07	3.32E-07	7.53E-07	6.88E-08	3.04E-07	1.84E-07
	$R_s(\Omega)$	0.03657	0.03610	0.03497	0.03477	0.04225	0.03616	0.03856
	$R_{sh}(\Omega)$	59.02188	51.32941	93.18672	88.58450	21.07085	56.53350	79.39953
	$n_1$	1.98726	1.47019	1.85900	1.73541	1.55271	2.00000	1.94919
	$n_2$	1.44652	1.94199	1.49112	1.60750	1.34104	1.47745	1.42947
RMSE	Best	<b>9.95E-04</b>	1.06E-03	2.06E-03	9.65E-03	5.83E-03	9.99E-04	1.98E-03
	Worst	<b>5.04E-03</b>	6.27E-03	6.31E-02	3.02E-01	9.64E-02	4.60E-02	1.14E-01
	Mean	<b>2.30E-03</b>	2.53E-03	1.83E-02	1.24E-01	3.46E-02	1.08E-02	2.94E-02
	Std	<b>7.70E-04</b>	7.93E-04	1.51E-02	6.67E-02	1.69E-02	1.46E-02	1.85E-02
wilcoxon-sign		3.99E-10	3.90E-18	3.90E-18	3.90E-18	2.22E-04	3.90E-18	

**Table 5.** IAE of IALA on DDM

Item	Measured data		Simulated current data		Simulated power data	
	V (V)	I (A)	$I_{sim}$ (A)	$IAE_I$ (A)	$P_{sim}$ (W)	$IAE_P$ (W)
1	-0.20570	0.76400	0.76370	0.00030	-0.15709	6.11E-05
2	-0.12910	0.76200	0.76241	0.00041	-0.09843	5.24E-05
3	-0.05880	0.76050	0.76122	0.00072	-0.04476	4.21E-05
4	0.00570	0.76050	0.76012	0.00038	0.00433	2.16E-06
5	0.06460	0.76000	0.75912	0.00088	0.04904	5.70E-05
6	0.11850	0.75900	0.75819	0.00081	0.08985	9.63E-05
7	0.16780	0.75700	0.75730	0.00030	0.12708	5.07E-05
8	0.21320	0.75700	0.75639	0.00061	0.16126	0.00013
9	0.25450	0.75550	0.75535	0.00015	0.19224	3.78E-05
10	0.29240	0.75400	0.75390	0.00010	0.22044	2.93E-05
11	0.32690	0.75050	0.75155	0.00105	0.24568	0.00034
12	0.35850	0.74650	0.74741	0.00091	0.26794	0.00032
13	0.38730	0.73850	0.74003	0.00153	0.28662	0.00059
14	0.41370	0.72800	0.72717	0.00083	0.30083	0.00034
15	0.43730	0.70650	0.70668	0.00018	0.30903	7.81E-05
16	0.45900	0.67550	0.67497	0.00053	0.30981	0.00025
17	0.47840	0.63200	0.63049	0.00151	0.30163	0.00072
18	0.49600	0.57300	0.57176	0.00124	0.28359	0.00062
19	0.51190	0.49900	0.49955	0.00055	0.25572	0.00028
20	0.52650	0.41300	0.41369	0.00069	0.21781	0.00036
21	0.53980	0.31650	0.31761	0.00111	0.17145	0.00060
22	0.55210	0.21200	0.21227	0.00027	0.11720	0.00015
23	0.56330	0.10350	0.10234	0.00116	0.05765	0.00065
24	0.57360	-0.01000	-0.00867	0.00133	-0.00497	0.00076
25	0.58330	-0.12300	-0.12555	0.00255	-0.07323	0.00149
26	0.59000	-0.21000	-0.20856	0.00144	-0.12305	0.00085
Sum of IAE				2.15E-02		8.97E-03



**Fig. 6.** Box-plot for the double-diode model

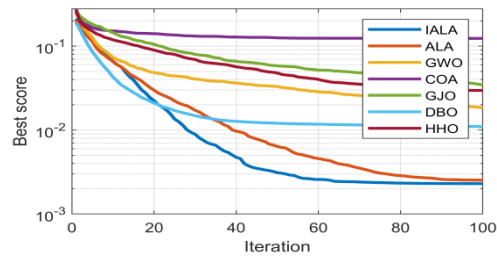


**Fig. 7.** Convergence performance of IALA and competing algorithms on the DDM model

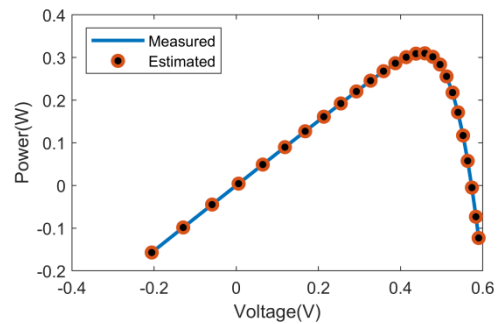
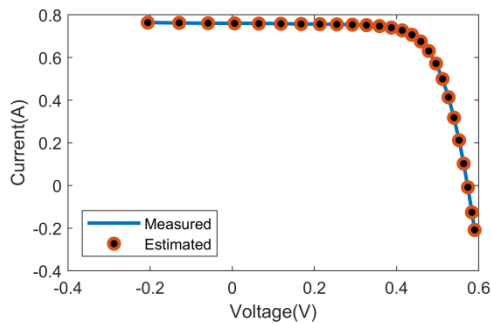


**Fig. 8.** The I-V and P-V characteristics of the DDM estimated by IALA

### 4.3 Results on the Three Diode Model

The optimal parameters for the three-diode model, along with the statistical outcomes of the optimization method, are shown in Table 6. Bold text indicates the ideal values. Fig. 9 shows a box plot of the RMSE distribution. Fig. 10 presents the convergence curves for each approach. The results demonstrate that IALA exhibits a stronger trend of converging to the optimal solution.

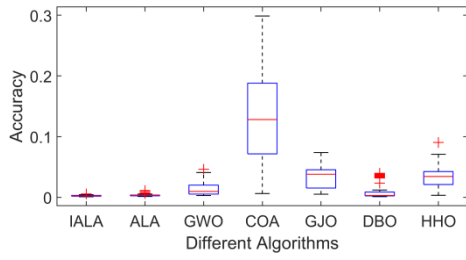
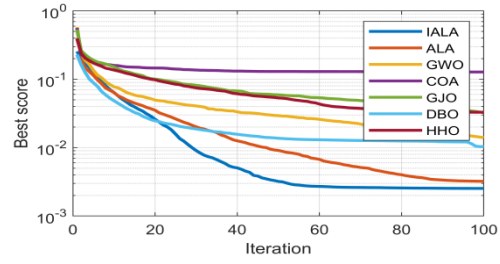
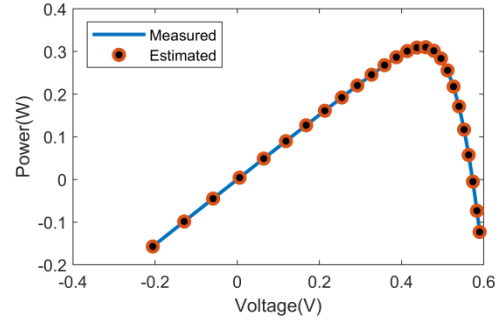
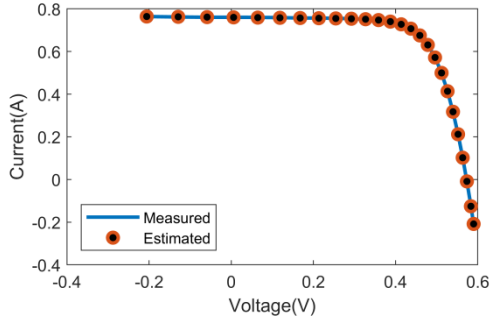
The IAE values for power and current are listed in Table 7, which makes it possible to assess how much the real values differ from the estimated findings. The cumulative IAE is  $8.59E-03$  for power and  $2.13E-02$  for current. Fig. 11 shows the observed and IALA-estimated I-V and P-V characteristics of the three-diode PV model. The close combination of simulation data and experimental data verifies the accuracy of the IALA algorithm.

**Table 6.** Results obtained for the TDM

Algorithm		IALA	ALA	GWO	COA	GJO	DBO	HHO
Best -obtained parameters	$i_{photo}(A)$	0.76075	0.75911	0.76134	0.76752	0.76594	0.76130	0.76006
	$i_{sd1}(\mu A)$	3.15E-07	1.42E-07	1.18E-07	9.57E-07	7.90E-07	1.00E-06	5.90E-07
	$i_{sd2}(\mu A)$	1.81E-19	4.40E-08	2.07E-08	4.73E-07	2.15E-07	8.07E-08	1.05E-07
	$i_{sd3}(\mu A)$	1.06E-19	1.00E-06	8.20E-07	5.18E-07	2.99E-07	1.00E-06	4.99E-07
	$R_s(\Omega)$	0.03649	0.03764	0.03125	0.03203	0.03209	0.03831	0.03110
	$R_{sh}(\Omega)$	53.72146	75.70169	78.87835	89.38225	75.56103	49.03096	61.65909
	$n_1$	1.47874	1.41460	1.90445	1.61662	1.71491	2.00000	1.55123
	$n_2$	2.00000	1.58480	1.82806	1.81085	1.98926	1.36583	1.92198
	$n_3$	2.00000	1.98489	1.58400	1.96728	1.51473	1.99873	1.95690
	RMSE	Best	<b>9.88E-04</b>	1.39E-03	2.94E-03	6.22E-03	5.14E-03	1.13E-03
Worst		<b>5.66E-03</b>	1.12E-02	4.61E-02	2.99E-01	7.38E-02	3.95E-02	9.04E-02
Mean		<b>2.53E-03</b>	3.22E-03	1.40E-02	1.28E-01	3.25E-02	1.03E-02	3.29E-02
Std		<b>9.22E-04</b>	1.47E-03	1.08E-02	6.91E-02	1.66E-02	1.36E-02	1.52E-02
wilcoxon-sign		5.67E-10	3.90E-18	3.90E-18	3.90E-18	3.23E-06	3.90E-18	

**Table 7.** IAE of IALA on TDM

Item	Measured data		Simulated current data		Simulated power data	
	V(V)	I(A)	$I_{sim}(A)$	$IAE_I(A)$	$P_{sim}(W)$	$IAE_P(W)$
1	-0.20570	0.76400	0.76406	6.39E-05	-0.15717	1.31E-05
2	-0.12910	0.76200	0.76264	0.00064	-0.09846	8.25E-05
3	-0.05880	0.76050	0.76133	0.00083	-0.04477	4.89E-05
4	0.00570	0.76050	0.76013	0.00037	0.00433	2.11E-06
5	0.06460	0.76000	0.75903	0.00097	0.04903	6.25E-05
6	0.11850	0.75900	0.75802	0.00098	0.08983	0.00012
7	0.16780	0.75700	0.75707	6.89E-05	0.12704	1.16E-05
8	0.21320	0.75700	0.75612	0.00088	0.16120	0.00019
9	0.25450	0.75550	0.75507	0.00043	0.19216	0.00011
10	0.29240	0.75400	0.75365	0.00035	0.22037	0.00010
11	0.32690	0.75050	0.75139	0.00089	0.24563	0.00029
12	0.35850	0.74650	0.74737	0.00087	0.26793	0.00031
13	0.38730	0.73850	0.74015	0.00165	0.28666	0.00064
14	0.41370	0.72800	0.72745	0.00055	0.30094	0.00023
15	0.43730	0.70650	0.70706	0.00056	0.30920	0.00025
16	0.45900	0.67550	0.67539	0.00011	0.31000	5.08E-05
17	0.47840	0.63200	0.63087	0.00113	0.30181	0.00054
18	0.49600	0.57300	0.57202	0.00098	0.28372	0.00049
19	0.51190	0.49900	0.49965	0.00065	0.25577	0.00033
20	0.52650	0.41300	0.41363	0.00063	0.21778	0.00033
21	0.53980	0.31650	0.31744	0.00094	0.17135	0.00050
22	0.55210	0.21200	0.21203	3.30E-05	0.11706	1.82E-05
23	0.56330	0.10350	0.10211	0.00139	0.05752	0.00078
24	0.57360	-0.01000	-0.00883	0.00117	-0.00507	0.00067
25	0.58330	-0.12300	-0.12557	0.00257	-0.07324	0.00150
26	0.59000	-0.21000	-0.20844	0.00156	-0.12298	0.00092
Sum of IAE				2.13E-02		8.59E-03


**Fig. 9.** Box-plot for the Three-diode model

**Fig. 10.** Convergence performance of IALA and competing algorithms on the TDM model

**Fig. 11.** Estimated I-V and P-V characteristics of the TDM using IALA

#### 4.4 Results on the Four Diode Model

Table 8 gives a comparison of the statistical results of the four-diode model calculated using several methods. These outcomes demonstrate that the suggested IALA algorithm outperforms alternative comparison algorithms. Furthermore, the consistent parameter estimation achieved by IALA for the four-diode model is clearly illustrated by the box plot in Fig. 12. Fig. 13 presents the convergence curves, demonstrating the effectiveness of IALA in avoiding stagnation and enhancing convergence speed. All current and power IAE values added together equal  $2.17E-02$  and  $8.97E-03$ , as shown in Table 9. The parameters derived from the IALA method show a high degree of agreement with the real experimental data, as shown in Fig. 14.

**Table 8.** Results obtained for the FDM

Algorithm		IALA	ALA	GWO	COA	GJO	DBO	HHO
Best -obtained parameters	$i_{photo}(A)$	0.76072	0.76000	0.76175	0.76443	0.75813	0.76115	0.76173
	$i_{sd1}(\mu A)$	1.85E-08	1.02E-07	0.00E+00	7.90E-08	0.00E+00	3.96E-07	3.72E-25
	$i_{sd2}(\mu A)$	1.57E-07	1.00E-06	2.63E-08	9.47E-07	0.00E+00	1.19E-07	4.79E-17
	$i_{sd3}(\mu A)$	1.01E-13	2.27E-07	3.59E-07	5.58E-08	2.90E-07	0.00E+00	2.98E-07
	$i_{sd4}(\mu A)$	3.40E-07	5.51E-07	6.85E-08	1.16E-07	7.54E-07	8.58E-07	1.49E-07
	$R_s(\Omega)$	0.03596	0.03528	0.03837	0.02943	0.02944	0.03831	0.03687
	$R_{sh}(\Omega)$	58.02632	99.70352	39.86204	29.71346	97.22573	46.98168	53.76316
	$n_1$	2.00000	1.94168	1.03809	1.51290	1.76717	2.00000	1.51038
	$n_2$	2.00000	1.99939	1.45783	1.63587	1.48002	1.39470	1.51256
	$n_3$	1.18510	1.45974	1.68271	1.58783	1.69495	1.00000	1.50983
$n_4$	1.48752	1.94425	1.36956	1.97371	1.59023	2.00000	1.52572	
RMSE	Best	<b>1.01E-03</b>	1.42E-03	1.49E-03	4.97E-03	4.26E-03	1.17E-03	3.78E-03
	Worst	<b>5.25E-03</b>	3.21E-02	5.60E-02	3.07E-01	7.53E-02	1.29E-01	8.90E-02
	Mean	<b>2.92E-03</b>	3.64E-03	1.68E-02	1.32E-01	3.59E-02	1.54E-02	3.33E-02
	Std	<b>9.65E-04</b>	3.06E-03	1.34E-02	6.31E-02	1.60E-02	2.35E-02	1.62E-02
wilcoxon-sign		7.13E-17	3.90E-18	3.90E-18	3.90E-18	5.18E-17	3.90E-18	

**Table 9.** IAE of IALA on FDM

Item	Measured data		Simulated current data		Simulated power data	
	V (V)	I (A)	$I_{sim}$ (A)	$IAE_I$ (A)	$P_{sim}$ (W)	$IAE_P$ (W)
1	-0.20570	0.76400	0.76379	0.00021	-0.15711	4.33E-05
2	-0.12910	0.76200	0.76247	0.00047	-0.09843	6.08E-05
3	-0.05880	0.76050	0.76126	0.00076	-0.04476	4.47E-05
4	0.00570	0.76050	0.76015	0.00035	0.00433	2.01E-06
5	0.06460	0.76000	0.75913	0.00087	0.04904	5.62E-05
6	0.11850	0.75900	0.75819	0.00081	0.08985	9.61E-05
7	0.16780	0.75700	0.75730	0.00030	0.12708	5.06E-05
8	0.21320	0.75700	0.75640	0.00060	0.16127	1.27E-04
9	0.25450	0.75550	0.75538	0.00012	0.19224	2.99E-05
10	0.29240	0.75400	0.75397	0.00003	0.22046	8.95E-06
11	0.32690	0.75050	0.75167	0.00117	0.24572	0.00038
12	0.35850	0.74650	0.74757	0.00107	0.26800	0.00038
13	0.38730	0.73850	0.74022	0.00172	0.28669	0.00066
14	0.41370	0.72800	0.72733	0.00067	0.30089	0.00028
15	0.43730	0.70650	0.70675	0.00025	0.30906	0.00011
16	0.45900	0.67550	0.67491	0.00059	0.30979	0.00027
17	0.47840	0.63200	0.63032	0.00168	0.30154	0.00080
18	0.49600	0.57300	0.57151	0.00149	0.28347	0.00074
19	0.51190	0.49900	0.49930	0.00030	0.25559	0.00016
20	0.52650	0.41300	0.41353	0.00053	0.21772	0.00028
21	0.53980	0.31650	0.31759	0.00109	0.17144	0.00059
22	0.55210	0.21200	0.21241	0.00041	0.11727	0.00022
23	0.56330	0.10350	0.10258	0.00092	0.05778	0.00052
24	0.57360	-0.01000	-0.00847	0.00153	-0.00486	0.00088
25	0.58330	-0.12300	-0.12547	0.00247	-0.07319	0.00144
26	0.59000	-0.21000	-0.20875	0.00125	-0.12316	0.00074
Sum of IAE				2.17E-02		8.97E-03

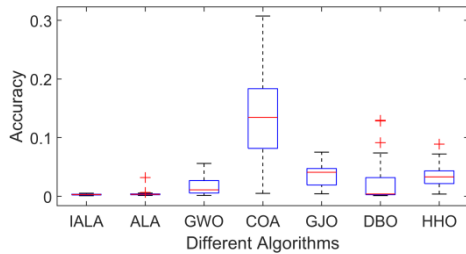


**Fig. 12.** Box-plot for the Four-diode model

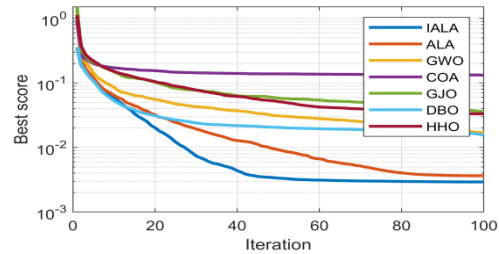


**Fig. 13.** Convergence performance of IALA and competing algorithms on the FDM model

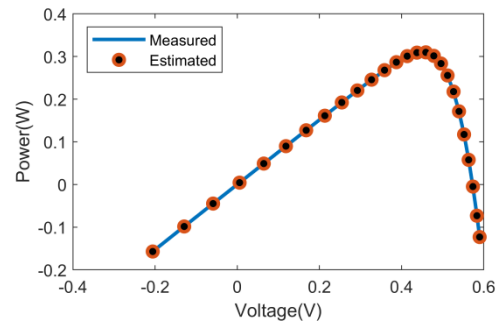
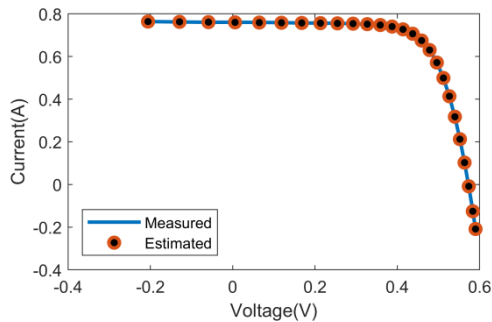


**Fig. 14.** The I-V and P-V characteristics of the FDM estimated by IALA

## 5 Conclusion

In order to improve the robustness of PV parameter extraction as model complexity increases, this paper presents IALA, an enhanced ALA technique. IALA uses a triangle walking strategy during the exploration phase to reduce the possibility of becoming trapped in local optima. Additionally, an inverse cumulative Cauchy distribution operator is introduced in the exploitation phase to speed up convergence to the optimal solution. The following findings can be made by contrasting IALA with other cutting-edge techniques for parameter extraction across four PV datasets:

As shown in Table 2-Table 9, IALA consistently achieves robust results, outperforming competing algorithms as the PV model complexity increases. The average convergence performance across all datasets demonstrates that IALA maintains a consistently fast descent speed throughout iterations, ensuring stable and reliable results in each run. In conclusion, it is demonstrated that the suggested IALA algorithm works well for identifying PV model parameters. Furthermore, its exploitation strategy may inspire advancements in other meta-heuristic algorithms.

## 6 Acknowledgement

The Natural Science Research Project of Anhui Province University, China (Grant Nos. KJ2021A1165 and 2023AH051814) and the Academic Funding Program for Top Talents in Higher Education Disciplines (Grant No. gxbjZD2022086) provided funding for this study.

## References

- [1] A.R. Jordehi, Parameter estimation of solar photovoltaic (PV) cells: A review, *Renewable and Sustainable Energy Reviews* 61(2016) 354-371.  
<https://doi.org/10.1016/j.rser.2016.03.049>
- [2] H. Saleem, S. Karmalkar, An Analytical Method to Extract the Physical Parameters of a Solar Cell From Four Points on the Illuminated J-V Curve, *IEEE Electron Device Letters* 30(4)(2009) 349-352.  
<https://doi.org/10.1109/LED.2009.2013882>
- [3] N. Maouhoub, Photovoltaic module parameter estimation using an analytical approach and least squares method, *Journal of Computational Electronics* 17(2)(2018) 784-790.  
<https://doi.org/10.1007/s10825-017-1121-5>
- [4] M.C. Di Piazza, M. Luna, G. Vitale, Dynamic PV Model Parameter Identification by Least-Squares Regression, *IEEE Journal of Photovoltaics* 3(2)(2013) 799-806.  
<https://doi.org/10.1109/JPHOTOV.2012.2236146>
- [5] A.R. Jordehi, Time varying acceleration coefficients particle swarm optimisation (TVACPSO): A new optimisation algorithm for estimating parameters of PV cells and modules, *Energy Conversion and Management* 129(2016) 262-274.  
<https://doi.org/10.1016/j.enconman.2016.09.085>
- [6] M.A. Abido, M.S. Khalid, Seven-parameter PV model estimation using Differential Evolution, *Electrical Engineering* 100(2)(2018) 971-981.  
<https://doi.org/10.1007/s00202-017-0542-2>
- [7] R. Bendaoud, H. Amiry, M. Benhmida, B. Zohal, S. Yadir, S. Bounouar, C. Hajjaj, E. Baghaz, M. El Aydi, New method for extracting physical parameters of PV generators combining an implemented genetic algorithm and the simulated annealing algorithm, *Solar Energy* 194(2019) 239-247.  
<https://doi.org/10.1016/j.solener.2019.10.040>
- [8] M. Merchaoui, A. Sakly, M.F. Mimouni, Particle swarm optimisation with adaptive mutation strategy for photovoltaic solar cell/module parameter extraction, *Energy Conversion and Management* 175(2018) 151-163.  
<https://doi.org/10.1016/j.enconman.2018.08.081>
- [9] H.M. Ridha, A.A. Heidari, M. Wang, H. Chen, Boosted mutation-based Harris hawks optimizer for parameters identification of single-diode solar cell models, *Energy Conversion and Management* 209(2020) 112660.  
<https://doi.org/10.1016/j.enconman.2020.112660>
- [10] D. Oliva, M. Abd El Aziz, A. Ella Hassanien, Parameter estimation of photovoltaic cells using an improved chaotic whale optimization algorithm, *Applied Energy* 200(2017) 141-154.  
<https://doi.org/10.1016/j.apenergy.2017.05.029>
- [11] O.S. Elazab, H.M. Hasanien, M.A. Elgendy, A.M. Abdeen, Parameters estimation of single- and multiple-diode photovoltaic model using whale optimisation algorithm, *IET Renewable Power Generation* 12(15)(2018) 1755-1761.

- <https://doi.org/10.1049/iet-rpg.2018.5317>
- [12] W. Long, S. Cai, J. Jiao, M. Xu, T. Wu, A new hybrid algorithm based on grey wolf optimizer and cuckoo search for parameter extraction of solar photovoltaic models, *Energy Conversion and Management* 203(2020) 112243. <https://doi.org/10.1016/j.enconman.2019.112243>
- [13] H. Chen, S. Jiao, M. Wang, A.A. Heidari, X. Zhao, Parameters identification of photovoltaic cells and modules using diversification-enriched Harris hawks optimization with chaotic drifts, *Journal of Cleaner Production* 244(2020) 118778. <https://doi.org/10.1016/j.jclepro.2019.118778>
- [14] H. Zhang, A.A. Heidari, M. Wang, L. Zhang, H. Chen, C. Li, Orthogonal Nelder-Mead moth flame method for parameters identification of photovoltaic modules, *Energy Conversion and Management* 211(2020) 112764. <https://doi.org/10.1016/j.enconman.2020.112764>
- [15] K. Sundareswaran, P. Sankar, P.S.R. Nayak, S.P. Simon, S. Palani, Enhanced Energy Output From a PV System Under Partial Shaded Conditions Through Artificial Bee Colony, *IEEE Transactions on Sustainable Energy* 6(1)(2015) 198-209. <https://doi.org/10.1109/TSTE.2014.2363521>
- [16] T.S.L.V. Ayyarao, G.I. Kishore, Parameter estimation of solar PV models with artificial humming bird optimization algorithm using various objective functions, *Soft Computing* 28(4)(2024) 3371-3392. <https://doi.org/10.1007/s00500-023-08630-x>
- [17] C. Janani, B.C. Babu, V. Krishnasamy, An accurate parameter estimation approach to modeling of solar photovoltaic module using hybrid grey wolf optimization, *Optimal Control Applications and Methods* 44(2)(2023) 601-616. <https://doi.org/10.1002/oca.2917>
- [18] Z. Garip, Parameters estimation of three-diode photovoltaic model using fractional-order Harris Hawks optimization algorithm, *Optik* 272(2023) 170391. <https://doi.org/10.1016/j.ijleo.2022.170391>
- [19] M.A. El-Dabah, R.A. El-Sehiemy, H.M. Hasanien, B. Saad, Photovoltaic model parameters identification using Northern Goshawk Optimization algorithm, *Energy*, 262 Part B (2023), 125522. <https://doi.org/10.1016/j.energy.2022.125522>
- [20] A. Słowik, K. Cpałka, Y. Xue, A. Hapka, An efficient approach to parameter extraction of photovoltaic cell models using a new population-based algorithm, *Applied Energy* 364(2024) 123208. <https://doi.org/10.1016/j.apenergy.2024.123208>
- [21] A.M. Shaheen, R.A. El-Sehiemy, G. Xiong, E. Elattar, A.R. Ginidi, Parameter identification of solar photovoltaic cell and module models via supply demand optimizer, *Ain Shams Engineering Journal* 13(4)(2022) 101705. <https://doi.org/10.1016/j.asej.2022.101705>
- [22] Y. Xiao, H. Cui, R.A. Khurma, P.A. Castillo, Artificial lemming algorithm: a novel bionic meta-heuristic technique for solving real-world engineering optimization problems, *Artificial Intelligence Review* 58(3)(2025) 84. <https://doi.org/10.1007/s10462-024-11023-7>
- [23] S. Liu, Triangular Walking Strategy Based Sand Cat Swarm Optimization for Color Level Determination in Visual Communication, in: *Proc. 2024 International Conference on Intelligent Algorithms for Computational Intelligence Systems (IACIS)*, 2024. <https://doi.org/10.1109/IACIS61494.2024.10721863>
- [24] M. Wang, J.-S. Wang, X.-D. Li, M. Zhang, W.-K. Hao, Harris Hawk Optimization Algorithm Based on Cauchy Distribution Inverse Cumulative Function and Tangent Flight Operator, *Applied Intelligence* 52(10)(2022) 10999-11026. <https://doi.org/10.1007/s10489-021-03080-0>
- [25] M. Ramachandran, A. Sundaram, H.M. Ridha, S. Mirjalili, Estimation of photovoltaic models using an enhanced Henry gas solubility optimization algorithm with first-order adaptive damping Berndt-Hall-Hall-Hausman method, *Energy Conversion and Management* 299(2024) 117831. <https://doi.org/10.1016/j.enconman.2023.117831>
- [26] N.M. Hatta, A.M. Zain, R. Sallehuddin, Z. Shayfull, Y. Yusoff, Recent studies on optimisation method of Grey Wolf Optimiser (GWO): a review (2014–2017), *Artificial Intelligence Review* 52(4)(2019) 2651-2683. <https://doi.org/10.1007/s10462-018-9634-2>
- [27] H. Jia, S. Shi, D. Wu, H. Rao, J. Zhang, L. Abualigah, Improve coati optimization algorithm for solving constrained engineering optimization problems, *Journal of Computational Design and Engineering* 10(6)(2023) 2223-2250. <https://doi.org/10.1093/jcde/qwad095>
- [28] N. Chopra, M.M. Ansari, Golden jackal optimization: A novel nature-inspired optimizer for engineering applications, *Expert Systems with Applications* 198(2022) 116924. <https://doi.org/10.1016/j.eswa.2022.116924>
- [29] M. Ye, H. Zhou, H. Yang, B. Hu, X. Wang, Multi-Strategy Improved Dung Beetle Optimization Algorithm and Its Applications, *Biomimetics* 9(5)(2024) 291. <https://doi.org/10.3390/biomimetics9050291>
- [30] A.A. Heidari, S. Mirjalili, H. Faris, I. Aljarah, M. Mafarja, H. Chen, Harris hawks optimization: Algorithm and applications, *Future Generation Computer Systems* 97(2019) 849-872. <https://doi.org/10.1016/j.future.2019.02.028>